



Research Article

miR-21 Responsive Nanocarrier Targeting Ovarian Cancer Cells



Liting Han^a, Tao Song^b, Xinyu Wang^a, Yan Luo^a, Chuanqi Gu^{a,b,c}, Xin Li^{a,*}, Jinda Wen^c, Zhibin Wen^c, Xiaolong Shi^c

^a Department of Gynecology 2, Renmin Hospital of Wuhan University, Wuhan, China

^b College of Computer Science and Technology, China University of Petroleum (East China), Qingdao, China

^c Institute of Computing Science and Technology, Guangzhou University, Guangzhou, China

ARTICLE INFO

Keywords:
DNA origami
Nano-drug
3D nanotube
MiR-21
Ovarian cancer
Cancer therapy

ABSTRACT

In recent years, DNA origami-based nanocarriers have been extensively utilized for efficient cancer therapy. However, developing a nanocarrier capable of effectively protecting cargos such as RNA remains a challenge. In this study, we designed a compact and controllable DNA tubular origami (DTO) measuring 120 nm in length and 18 nm in width. The DTO exhibited appropriate structural characteristics for encapsulating and safeguarding cargo. Inside the DTO, we incorporated 20 connecting points to facilitate the delivery of cargoes to various ovarian and normal epithelial cell lines. Specifically, fluorescent-labeled DNA strands were attached to these sites as cargoes. The DTO was engineered to open upon encountering miR-21 through RNA/DNA strand displacement. Significantly, for the first time, we inhibited fluorescence using the compact DNA nanotube and observed dynamic fluorescent signals, indicating the controllable opening of DTO through live-cell imaging. Our results demonstrated that the DTO remained properly closed, exhibited effective internalization in ovarian cancer cells *in vitro*, showcasing marked differential expression of miR-21, and efficiently opened with short-term exposure to miR-21. Leveraging its autonomous behavior and compact design, the DTO emerges as a promising nanocarrier for various clinically relevant materials. It holds significant application prospects in anti-cancer therapy and the development of flexible biosensors.

1. Introduction

Delivery systems based on a wide range of materials have been developed for cancer therapy [1]. Notably, substantial research efforts have been dedicated to nanotechnology, aiming to construct universal carriers capable of transporting and protecting multiple functional agents. Three dimensional nanodevices constructed via DNA origami have garnered considerable research interest owing to their high compatibility, low toxicity, and biomedical potential. DNA is considered as the prospective material for self-assembly, attributed to its high predictability, hybridization dynamicity, strict and reliable complementary compatibility, arbitrary artificial composability, and stability. These characteristics are crucial in designing long-lasting biomaterials, making DNA a unique molecule suitable for programming self-assembling nanostructures with specific geometries [2].

Since its inception by Rothemund in 2006, DNA origami has evolved into a versatile platform in structural DNA nanotechnology, gaining increased attention with advancements in atomic force microscopy

(AFM) [3,4]. In recent years, different forms of 2D and 3D DNA origami structures have been developed as delivery systems [5,6]. The cellular uptake of versatile DNA structures, such as triangles [7,8], tetrahedra [9], cubes [10], and cages [11], have been demonstrated both *in vitro* and *in vivo*. However, few of these delivery systems possess inherent cargo protection, with most requiring additional wrapping materials. Therefore, there is a need to develop carriers that are inherently protective.

The DNA tubular structure represents one of the fundamental 3D nanostructures. Inspired by the roles of microtubules in cell structure support (e.g., actin filaments), intracellular trafficking (e.g., microtubules), and cell motility (e.g., flagella), DNA nanotubes could be precisely programmed to simulate these functions through DNA origami. Moreover, DNA nanotubes have attractive biophysical properties that allow for simpler control of their structure, energy, and kinetics compared to those of protein monomers [12]. Consequently, many studies have used DNA nanotubes to deliver drugs and other materials [13,14]. Furthermore, a groundbreaking design strategy for

* Corresponding author.

E-mail address: xin.li@whu.edu.cn (X. Li).

dynamically switching origami is receiving increasing research interest. Flexible origami plays a critical role in the assembly of molecular machines [15]. Ketterer et al. devised a nanomolecular motor composed of diverse nanotube structures capable of nanoscale rotation. Self-assembled nanotubes exhibit outstanding potential across various applications, ranging from nanofabrication to biophysical research [16–18]. In 2013, Mohammed et al. demonstrated the achievement of a tubular structure by applying tension for the curling of a flat rectangular origami into a tubular form, using complementary DNA sequences extending from the staple strands at the top and bottom of the origami structure [19]. Additionally, it is feasible to create dynamic origami with stimulus-triggered reconfiguration, allowing for controllable therapeutic release in targeted applications.

In this study, we designed a highly compact controllable nanoscale DNA tubular origami (DTO) that responds to intracellular microRNA-21 (miR-21) activity. miRNAs play roles in almost all aspects of cancer development [20], and miR-21 is one of the earliest and most well-known "oncomirs" that negatively affects various cellular functions associated with signaling pathways, including cell cycle, migration, and proliferation. Abnormal expression of miR-21 has been observed in numerous tumor cells, indicating its crucial role in tumor occurrence and progression [21–24]. Ovarian cancer, particularly epithelial ovarian cancer, represents the most lethal malignant gynecological tumor with a higher mortality rate despite its lower incidence compared to other cancers like endometrial cancer [25–27]. Previous studies have shown upregulated expression of miR-21 in ovarian cancer [28,29]. Additionally, miR-21 regulates the proliferation and apoptosis of ovarian cancer cells by modulating the PTEN/PI3K/AKT pathway [30]. Therefore, by designing miR-21-dependent nanodevices, there exists the potential to enhance the efficacy of targeted therapies in cancer cells and reduce side effects.

In this study, we designed a miR-21-responsive nanotube structure as a nanocarrier to ovarian cancer cells (Fig. 1). Intracellular miR-21 served as a "key" to unlock the closed nanotube through chain replacement; it competitively combined with a portion of the sealing chains to form a more stable double-stranded complex, thereby breaking the seal and causing the DTO to open. Additionally, research has demonstrated that the binding between DNA and RNA is the most stable, exhibiting lower free energy compared to DNA-DNA and RNA-RNA interactions [31]. In our study, live cell imaging was used for the first time to study the cellular internalization and switching characteristics of any controllable nanostructure. The DTO exhibited superior material and morphological properties. As a nanocarrier, the DTO rapidly opens upon stimulation by endogenous miRNA. It not only protects internal materials from enzymatic degradation but also enables precise and controllable switching to the open state. The DTO emerges as a promising candidate for treatment modalities, holding significant potential in anticancer therapy and serving as a versatile biosensor in the development of effective nanodrugs.

2. Materials and methods

2.1. Materials and reagents

All staple strands, including those with linker extensions, were purchased from Sangon Biotech (Shanghai, China), purified via high affinity purification (HAP), and diluted to a final concentration of 100 μ M in 1 \times TAE (Tris, Acetic acid, EDTA) buffer with 12.5 mM Mg^{2+} . The FAM (Fluorescein maleimide)-modified DNAs were purified by high performance liquid chromatography (HPLC). M13mp18 was obtained from New England Biolabs (NEB, Massachusetts, USA). Ultrafiltration centrifugal tubes were purchased from Millipore Sigma (Burlington, MA,

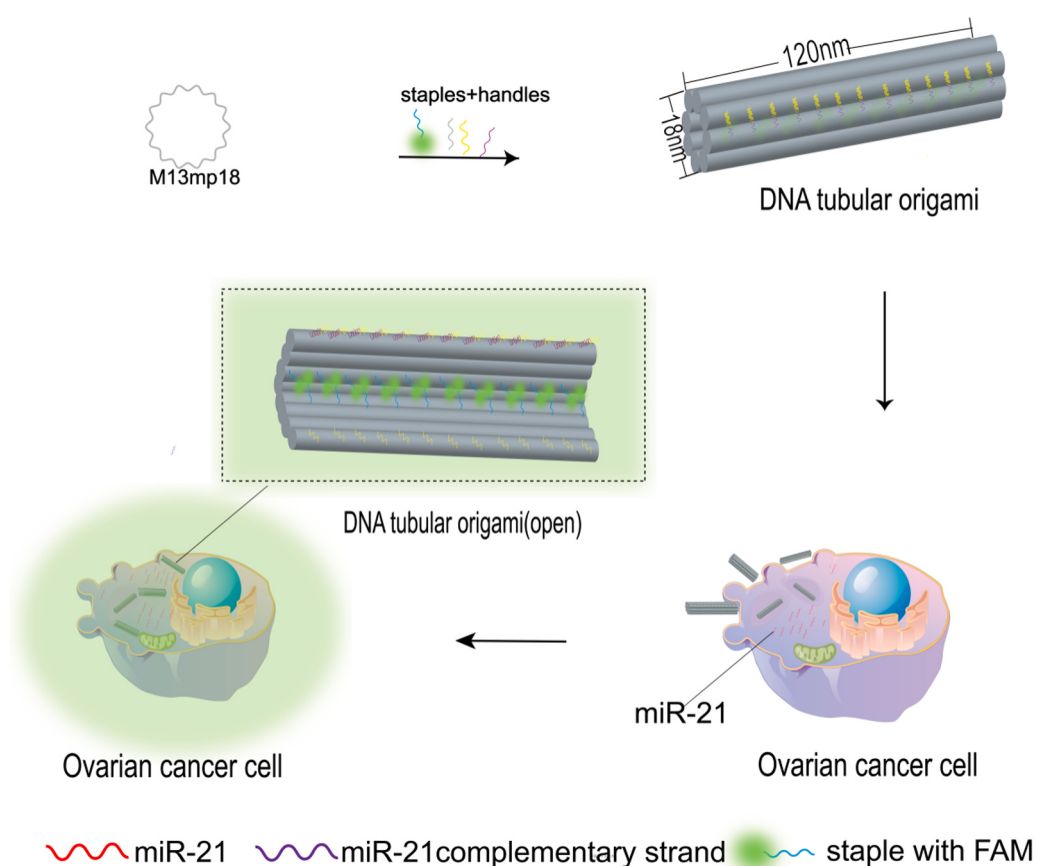


Fig. 1. Schematic representation of the preparation of the DNA tubular origami (DTO) and its application in ovarian cancer cells.

USA). Human ovarian cancer cell lines (SKOV3/DDP, A2780, A2780/DDP, COC1) and a normal ovarian epithelial cell line (IOSE80) were purchased from the China Center for Type Culture Collection (CCTCC, Wuhan, China). Fetal bovine serum (FBS) and RPMI 1640 medium were bought from Gibco (Shanghai, China). Total RNA was extracted using TRIzol (Solarbio, Beijing, China), chloroform, and isopropanol. RNase-free water was used in all RNA-related experiments. A miRNA Reverse Transcription Kit and 2 × SYBR Green qPCR master mix were supplied by Sangon Biotech.

2.2. Methods

2.2.1. Structure design

A half-roll origami was created using the square lattice module of caDNAno (<http://cadnano.org>) [32]. 104 staple strands were used to bind M13mp18 strands into an 8-helix rectangular origami. We have left quite a bit of the M13mp18 scaffold unhybridized, and the site of the unhybridized sections were shown in Fig. S1. Additionally, the folding structure was spontaneously coiled and molded into a curved shape by adding insertions and deletions based on Winfree's work [33]. In their design, the three adjacent spirals form a certain angle by changing the torsion degree, ultimately constructing the tubular structure. However, the designed structure can curl completely into a tubular shape which cannot be opened and closed flexibly. This would require the intelligent system to rely solely on biodegradation to unlock the structure. Therefore, this study aims to address these issues.

To seal the edges of the origami, "zippers" composed of two complementary DNA strands attached to the top and bottom helices respectively were introduced in our DNA tubular origami (DTO), and one of them was complementary to miR-21 (UAGCU UAUCA GACUG AUGUUU GA), the sequence is TCAACATCAGTCTGATAAGCTA with toehold (TGATAAGCTA) incorporated. Upon entering the cell, intracellular miR-21 initiates a strand displacement reaction that competitively combined with "zippers", resulting in the controlled release of the cargoes. Due to insufficient torsion force between the spirals, DTO does not remain in a coiled tubular state, allowing the cargoes attached to its inner walls to be fully exposed to the cytoplasm.

Furthermore, thermodynamic simulation was performed using CanDo, an auxiliary tool that mimics the actual structures constructed by caDNAno and allows for the computational analysis of the DTO. The front and lateral views are depicted in Fig. 2B. According to the thermodynamic stability simulation, the middle of the origami is more stable, so we chose 20 staples in the middle of the DTO as the connection points, which will remain stable when rolled into a tubular state.

2.2.2. Preparation of the DTO

The M13 scaffold and staple strands were mixed at final concentrations of 5 nM and 50 nM in 1 × TAE(12.5 mM Mg²⁺), respectively (1:10 ratio). The mixed solution was then subjected to the following thermal annealing program: 95 °C for 5 min, and then a linear cooling from 95 °C to 4 °C at a rate of 1 °C per minute. All oligonucleotides are listed

in Table S1.

2.2.3. Purification of the DTO

We used 100 kDa ultrafiltration tubes (Millipore, Sigma) to purify and concentrate the samples. The inner areas of the ultrafiltration tubes were moistened with 1 × TAE buffer until use. The samples were centrifuged at 12 000 rpm (revolutions per minute) for 5 min at 4 °C by an ultra-fast refrigerated centrifuge (Pingfan Technology Co., Ltd, China). The inner tube was then inverted and inserted into a new microcentrifuge tube, allowing the concentrated sample without free strands to be transferred to the new collection tube.

2.2.4. Gel electrophoresis

Agar (0.4 g) was added in 50 mL Tris acetate EDTA (1 × TAE) with 12.5 mM Mg²⁺ to make a 0.8% agarose gel (GelRed-stained, running buffer: 1 × TAE with 12.5 mM Mg²⁺). Samples were prepared to a concentration of 20 nM and 10 μL samples were mixed with 6 × DNA loading buffer (bromophenol blue in it) at a ratio of 5:1. Agarose gel electrophoresis was performed at a constant voltage of 90 V for 50 min. Finally, the bands were visualized and photographed using Protein Simple (Bio-Techne, San Jose, CA, USA).

2.2.5. Characterization of the DTO using atomic force microscopy

AFM scanning was conducted using a Multimode 8 serial atomic force microscope (Bruker Corporation, Billerica, MA, USA). The sample (10 μL) was dropped onto freshly prepared mica and retained for 10 min for adsorption before microscopic observation.

2.2.6. Transmission electron microscopy characterization of the DTO

A 5 μL sample was spotted onto a carbon-coated copper grid and left to adsorb for 10 min. Then, 2 μL 3% uranyl acetate was used to stain the grid for 1–2 min. And drain the solution from the copper mesh from the side with filter paper. 2 μL 3% uranyl acetate was used again to stain the grid for 30 s. The grid was left to dry overnight before performing TEM using a Talos F200C instrument (Thermo Fisher Scientific, Waltham, MA, USA).

2.2.7. Fluorescence measurement

First, the M13 scaffold, staple, and handle strands labeled fluorescein (FAM) were annealed at final concentrations of 5 nM, 50 nM, and 2000 nM, respectively (1:10:400), using the "one-pot" method. The annealing protocol was the same as that used to assemble the single tubular origami structure without handle strands. The experimental and control groups were concentrated using a 100 kDa ultrafiltration step. A 20 μL sample with excessive unlabeled strands (mimicking miR-21), served as a "key" to open the sealing of the DTO, was used to performed an unzipping experiment, while the control group did not contain unlabeled strands. Finally, the experimental and control samples were analyzed by quantitative real-time PCR (qPCR).

We applied a second protocol that required two ultrafiltration enrichment steps. First, two samples of origamis without handle strands



Fig. 2. Thermodynamic simulation diagrams of the DNA tubular origami (DTO);(A) In the traditional method without "insertion" and "deletion" operations;(B) With "insertion" and "deletion" operations in our study.

were prepared using the method as described above. Second, the two groups were enriched using a 100 kDa ultrafiltration step to remove the redundant free staple strands. Then, handle strands labeled FAM were added at a 40-fold excess concentration (40 nM) over the scaffold (i.e., 1 nM) into the sample. After maintaining the sample at 37 °C in the PCR instrument for 30 min, the temperature was reduced to 15 °C at a rate of 2 °C per min and then kept at 20 °C, and thus the handle labelled FAM was connected with DTO. To remove interference from the free handle strands labelled with FAM, the two groups were enriched again through a 100 kDa ultrafiltration step. Similar as in the first method, the unzipping experiment was performed and the experimental and control samples were analyzed using qPCR.

Fluorescence was measured in two groups, DTO groups with and without unlined strands (mimicking miR-21), at an incubation temperature of 25 °C (room temperature) for 100 min.

2.2.8. Cell culture and RT-qPCR

The cells were cultured in RPMI 1640 complete medium (containing 10% FBS, 100 U/mL penicillin–streptomycin solution) in a 5% CO₂ atmosphere at 37 °C.

All tips and microcentrifuge tubes used for the RNA experiments were RNase-free. Total RNA was extracted from the cells using TRIzol reagent, according to the manufacturer's instructions. The concentration of RNA in each sample was detected using an Ultramicro Spectrophotometer (Kai Ao, China). To reverse transcribe the RNA samples to cDNA, the microRNA Reverse Transcription Kit was used. PCR was performed using a MicroRNAs qPCR Kit (Sangon, China). Target gene amplification was performed using a real-time PCR platform (Bio-Rad Laboratories, Hercules, CA, USA) with the miR-21 forward primer (5'-CCGCTCGTAGCTTATCAGACTG-3') and a universal reverse primer from the MicroRNAs qPCR Kit. The mRNA level of target genes was normalized to that of *U6*, and the relative fold-change was calculated using the $\Delta\Delta Ct$ method.

2.2.9. Flow cytometry

The cells were seeded on a plastic-bottom 6-well plate and cultured for 24 h. Afterwards, they were incubated with DTO, whose inner wall was attached with FAM-labelled handle strands and pre-diluted with RPMI 1640 to a final concentration of 100 nM (600 μ L) for 0.5 h, 1 h, 2 h, and 3 h in full media. Subsequently, the cells were washed with PBS twice, treated with trypsin, collected, and gently resuspended in 200 μ L PBS. The fluorescence intensity of FAM was measured with a Beckman CytoFLEX (Beckman Coulter, Indianapolis, IN, USA) by counting 15,000 events in the FITC channel.

2.2.10. Live cell imaging of the intracellular uptake of DTO

SKOV3/DDP and A2780/DDP cells (5×10^3) were cultured in a 35-mm confocal dish with a glass bottom (Biosharp, Hefei city, China) overnight, and were incubated with DTO carrying Cy3 (50 nM) diluted with RPMI 1640 at 37 °C and 5% CO₂. Real-time fluorescence was conducted using a Zeiss ultra-high resolution inverted laser confocal microscope (LSM880, Zeiss, Oberkochen, Germany). SKOV3/DDP, A2780/DDP and IOSE80 cells were then incubated with DTO-Cy3 (50 nM) diluted with RPMI 1640 for 10 h at 37 °C, washed with PBS, fixed with 4% paraformaldehyde for 15 min, and stained with DAPI (Solarbio) for 20 min. After treatment with each reagent, the cells were washed three times with PBS and imaged with the laser confocal microscope.

3. Statistical analysis

All data are represented as the mean \pm standard deviation (SD) of three independent measurements. Statistical analyses were performed using GraphPad Prism software (version 8.0, for Windows, GraphPad Software, San Diego, CA, USA). Differences between groups were analyzed using a one-way ANOVA and two-tailed unpaired *t*-test.

Significance was set at $P < 0.05$.

4. Results and discussion

4.1. Synthesis and characterization of DTO

Since the development of DNA origami, there have been numerous studies focused on nanotubes. There are two issues with traditional strategies in this regard. Firstly, the formed twists result in uncontrolled structure. Even with the addition of nano-device locks, it is difficult to control the direction of the twists in the folded structure, potentially leading to biofunctional groups being attached to the outer wall of the tube. Secondly, this design may cause mismatches in staple strands extending from the longer sides of rectangular structures, resulting in misalignment of the opposing edges rather than achieving a perfect edge-to-edge connection (Fig. 2A).

Here, our DTO is a 3D nanostructure with a total of 104 staple strands: 84 for the main body of the DTO, and 26 of them were pre-designed to seal the origami on two sides of the edge. Another 20 staple strands functioned as signal or cargo binding sites. We added handle strands labeled FAM fluorescence that can connect with the 20 sites. Through the "one-pot" method, the DTO was synthesized by complementary pairing between the bases. Before observing the microstructure of the tubular origami, its formation was preliminarily verified by agarose gel electrophoresis (Fig. 3 A). To confirm the structural features, the prepared origami samples were pipetted onto a transparent mica sheet; Fig. 3B shows a representative AFM image of a closed tubular origami, and the length is about 120 nm (Fig. S2), and this may affect their enrichment at the tumor site due to enhanced permeability and retention (EPR) effects according to the morphology of DTO [34]. Surprisingly, the measured width of the DTO was 18 nm, which is irreconcilable with the theoretical width of 10.8 nm. Considering that DNA origami samples placed on mica in the process of resting on the mica will be somewhat flattened on the mica surface due to the electrostatic forces on the surface of the mica, the actual observed width of the tubular structure should be between 4 helices and 8 helices. This is due to the low torsional deformation force of the origami structure of the design, as well as the long cross sequence of the staple chain between the top and bottom structures of the design that does not create an overly strong tensile force. We determined the cylindrical conformation using TEM. A representative image of the closed DTO is shown in Fig. 3 C. Given that the marking errors during measurement, the actual width measured was 13 nm, which is within the acceptable range.

Consistent with the measurement, the opening of the DTO was verified through AFM (Fig. 4 A) after executing an unzipping experiment. The theoretical width of the origami structure was anticipated to be 21.6 nm, yet it exhibited inconsistency with the measured width (~60 nm). Notably, a distinct dividing line with low height was observed in the middle of the origami, and both edges of the origami maintained the same height. This phenomenon could be attributed to the dimerization of two opened origami structures induced by the complementary pairing of sealing chains (Fig. 4B). Representative AFM images of the DTO stored in a closed state for 1.5 days or longer are presented in Fig. 4 C and 4D. Although the origami structure exhibited some degradation, the two origamis did not form interconnections. This observation indicates that in the absence of free staples at the upper and lower edges of the DTO, the DTO does not aggregate to form connections. These findings unequivocally confirm the successful synthesis of our DTO.

4.2. Fluorescence measurement of DTO response to miR-21

Following the successful fabrication of the DTO, a fluorescence experiment was performed to quantify the internal fluorescence of DTO exposed to unlined strands (mimicking miR-21). Based on Xue et al. [35], it is feasible to represent the miR-21 responsive phenotype in the

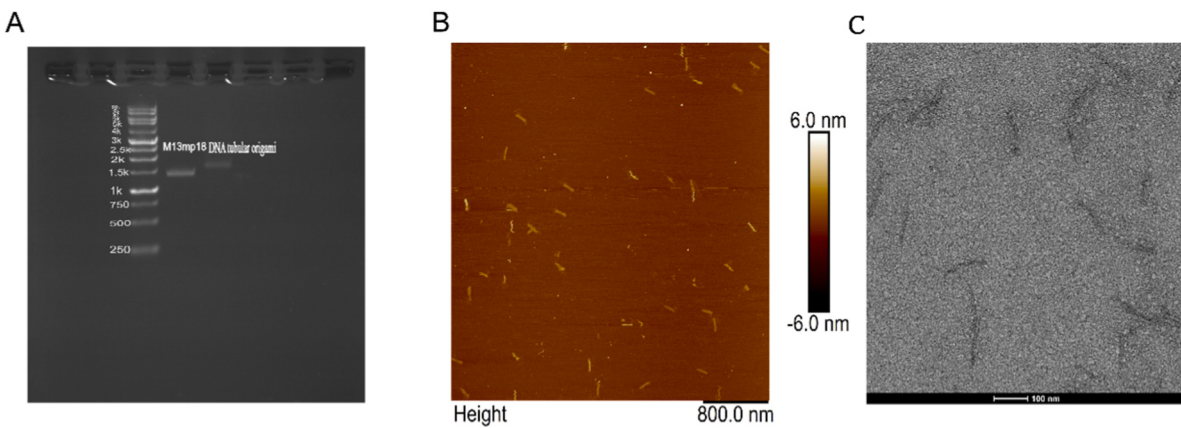


Fig. 3. (A) Agarose gel electrophoresis image of the DTO; (B) Atomic force microscopy imaging of the half-rolled DNA tubular origami. Scale bar: 800 nm;(C) Transmission electron microscopy of the closed DNA tubular origami. Scale bar: 100 nm.

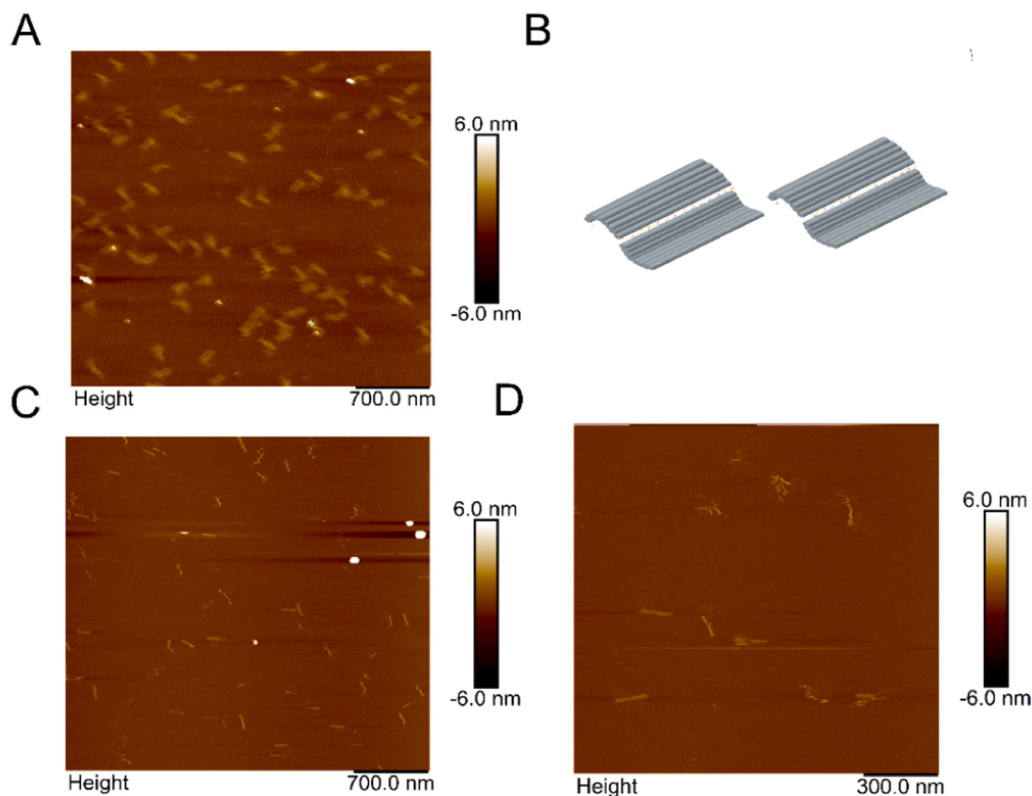


Fig. 4. (A) Atomic force microscopy imaging of the DTO in open state; (B) Diagram of two DTO cross-linked to each other in open state; (C) and (D) Atomic force microscopy imaging of the DTO in the closed state for more than 1.5 days. Scale bar: (A) 700 nm, (C) 700 nm, and (D) 300 nm.

hypothetical optimum state by tracking changes in fluorescence intensity. We compared two synthetic methods. In the two-ultrafiltration enrichment-step method, the handles labeled FAM were added in the second step without changing the morphology of the DTO. In our work, both staple strands and handle strands were in excess, leading to the assumption that all M13 was bound, and the excess strands were subsequently filtered out. Given that there are 20 binding sites per origami, the concentration of FAM-labeled handle strands bound to the DTO was 20 times that of M13. Fig. 5A illustrates the results of the one-pot experiment and the double ultrafiltration enrichment method. Following previous research, an incubation temperature of 50 °C was initially chosen and maintained for 12 h, ensuring the unzipping of the DTO. Subsequently, fluorescence detection occurred at a constant temperature of 6 °C, at which the DTO is stable. Fluorescence readings were

collected every 10 s for a total of 100 times [33]. As depicted in the experimental diagram (Fig. 5 A), the fluorescence values of the opened DTO were significantly higher than those of the closed ones. After two ultrafiltration steps, the free fluorescence was notably reduced. After two ultrafiltration steps, the free fluorescence was significantly reduced. To simulate the cellular uptake of the DTO under experimental conditions, the real-time fluorescence signal intensities of two groups are presented in Fig. 5B, conducted at room temperature. The experimental group exhibited a much higher fluorescence intensity than the control group, with almost no fluorescence detected in the control group, indicating the effective closure of our DTO. These results suggest that both approaches can effectively synthesize DTO, and it can be promptly opened by miR-21.

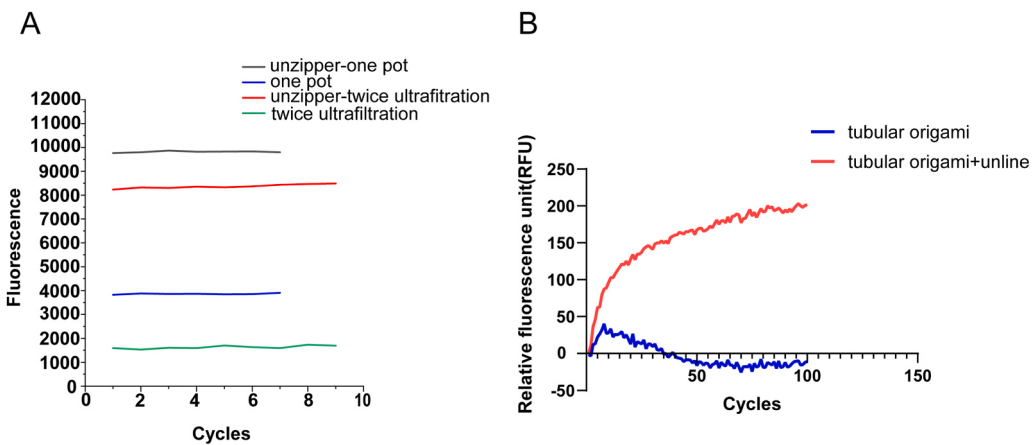


Fig. 5. (A)Fluorescence analysis at 6 °C after 12 h of incubation at 50 °C.(B)Real-time fluorescence quantitative analysis at 25 °C.

4.3. Expression of miR-21 in ovarian cancer cell lines

Numerous studies have consistently reported the overexpression of miR-21 in various tumor tissues, highlighting its role in promoting the occurrence and progression of tumors [36,37]. Moreover, miR-21 has been identified as a significant contributor to M2 macrophage-mediated chemoresistance in ovarian cancer cells [38]. Given its pivotal role as the "key" to open our DTO, it is imperative to measure the expression level of miR-21 in different ovarian cancer cell lines and normal ovarian epithelial cells (IOSE80). The results of fluorescence quantitative PCR are presented in Fig. 6, revealing that the highest miR-21 expression levels were observed in SKOV3/DDP and A2780/DDP cells. Consequently, SKOV3/DDP and A2780/DDP cells were selected for subsequent experiments.

4.4. Flow cytometry of intracellular uptake

The cellular uptake efficiency of the DTO in different cell lines was then examined by flow cytometry, which can provide fluorescent statistics for a large cell population and avoid errors caused by individual differences in a small number of cells. It was previously demonstrated that larger and more compact DNA origami structures can be more efficiently phagocytosed by cells than single DNA strands or simple

structures [39]. In Seung-Hyeon's study, their DNA nanotubes showed significant fluorescence after just one hour of incubation with KB cells [40]. Next, we treated the A2780/DDP, SKOV3/DDP, and IOSE80 cells with DTOs internally loaded with FAM-labeled handle (100 nM) for 0.5 h, 1 h, 2 h, and 3 h. FAM fluorescence in the FITC channel was analyzed by flow cytometry three times for each sample, and 15,000 events were counted. A2780/DDP cells showed increased fluorescence intensity compared with that in the untreated cells after 0.5 h (Fig. 8 A). However, there was no significant change in fluorescence intensity with longer incubation time. SKOV3/DDP cells showed a time-dependent increase in fluorescence intensity, but this was lower than that of A2780/DDP cells under the same conditions, which may be due to the different uptake efficiencies of the cell lines [41]. We did not detect any fluorescence signal in the IOSE80 cells within 3 h, as expected. And COC1 showed similar results as well. (Fig. S3)Fig. 7B presents the quantitative fluorescence intensity of each sample in Fig. 7 A. These results demonstrated that our DTO nanodevice can be internalized within a short time and effectively opened up by miR-21.

4.5. Live-Cell imaging of intracellular uptake

In recent years, live-cell imaging technology has revolutionized research because of its high resolution and dynamic precision. To overcome the potential quenching of FAM fluorescence, Cy3 fluorophore was labeled onto the DTO (handle strands), allowing the tracking of cellular uptake through confocal microscopy. The A2780/DDP and SKOV3/DDP cells were observed in real time at 37 °C in 5% CO₂ using the Zeiss laser confocal live cell imaging system. Images were captured from the time the DTO was added to the appearance of fluorescence in 0.5 h (Fig. 8 A). A2780/DDP cells showed high fluorescence intensity, while SKOV3/DDP cells exhibited very weak fluorescence. This result is consistent with the flow cytometry analysis, which suggests that DTO can rapidly and efficiently aggregate to the cell membrane. After three hours of incubation, both A2780/DDP and SKOV3/DDP exhibited intense red fluorescence (Cy3), indicating effective uptake, while fluorescence in IOSE80 was barely observable (Fig. 8B). And we can see that it has entered the cell within 3 h. This suggests that the DNA nanoscale structures we designed may have a relatively fast cellular uptake rate. In the subsequent experiment, we illustrated the intracellular localization of DTO in the A2780/DDP, SKOV3/DDP, and IOSE80 cells incubated with DTO-Cy3 for longer time of 10 h, and dyed with DAPI, which can specifically label the nucleus. And then they were fixed with 4% paraformaldehyde. After scanning at multiple levels of the cell, a red fluorescence signal was detected in all cell lines but in different areas (Fig. 8 C). In the IOSE80 cells, nearly all the fluorescence was clustered at the cell membrane. This may be due to the lack of strong and effective targeting of our DTO and the presence of a small amount of

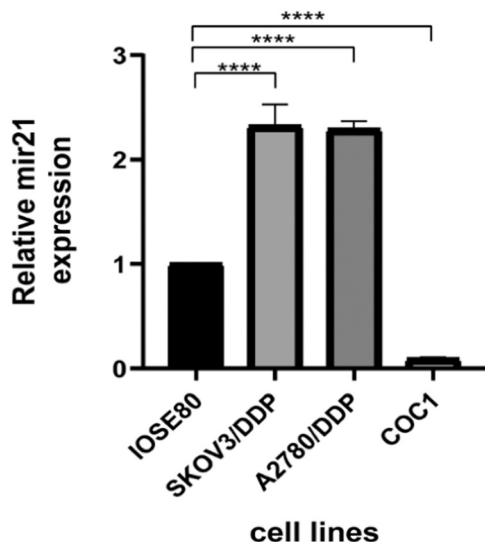


Fig. 6. Relative expression analysis of miR-21 in IOSE80, SKOV3/DDP, A2780/DDP, and COC1 cell lines. Results were compared using a two-tailed unpaired t-test. (****p < 0.0001, IOSE80 vs SKOV3/DDP, A2780/DDP, and COC1).

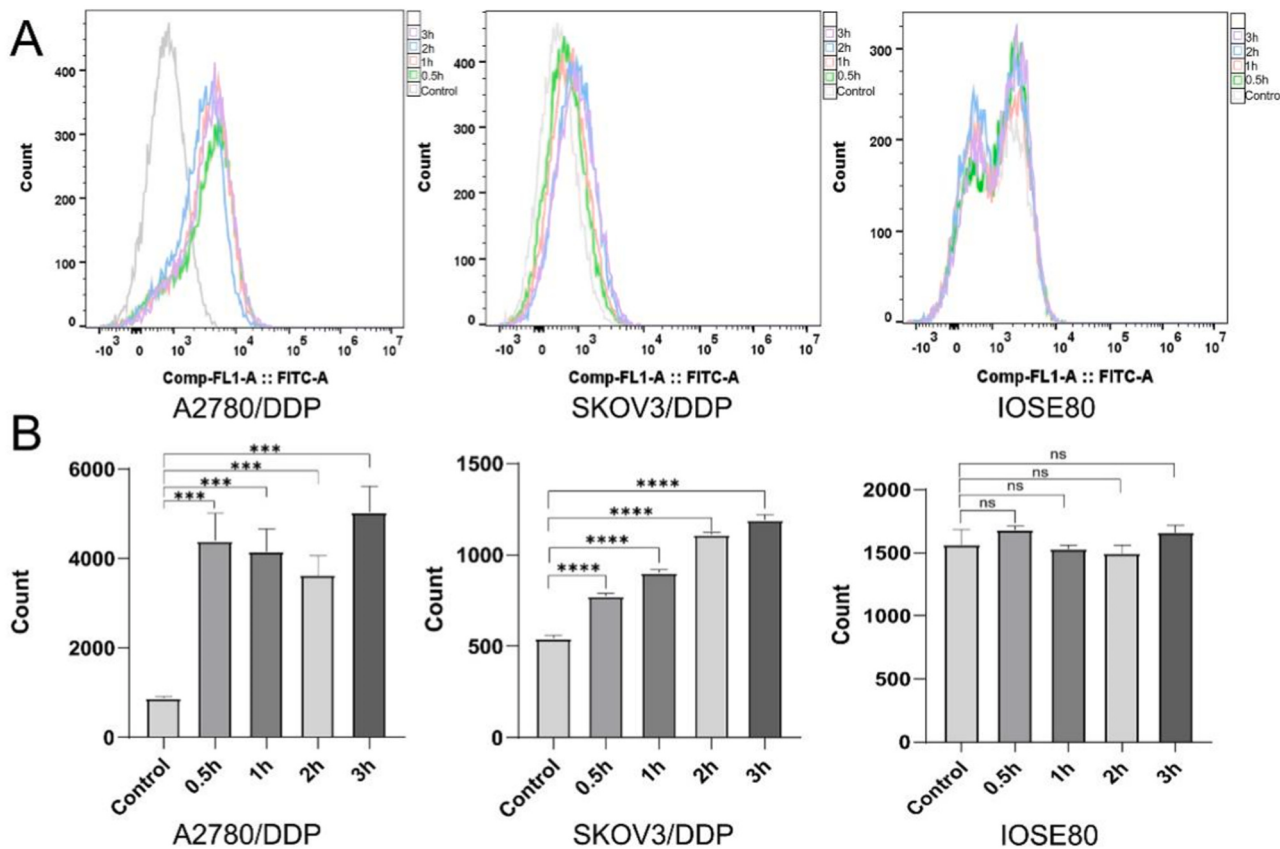


Fig. 7. (A) Flow cytometry analysis of A2780/DDP, SKOV3/DDP, IOSE80 cells treated with DTO-FAM (100 nM) for 0.5 h, 1 h, 2 h, 3 h, respectively; (B) The quantitative fluorescence intensity of each sample in A. (The data are presented as means \pm SDs, $n = 3$, the following P values were used to determine statistical significance: ns, $P > 0.05$; *, $P < 0.05$; **, $P < 0.01$ and ***, $P < 0.001$).

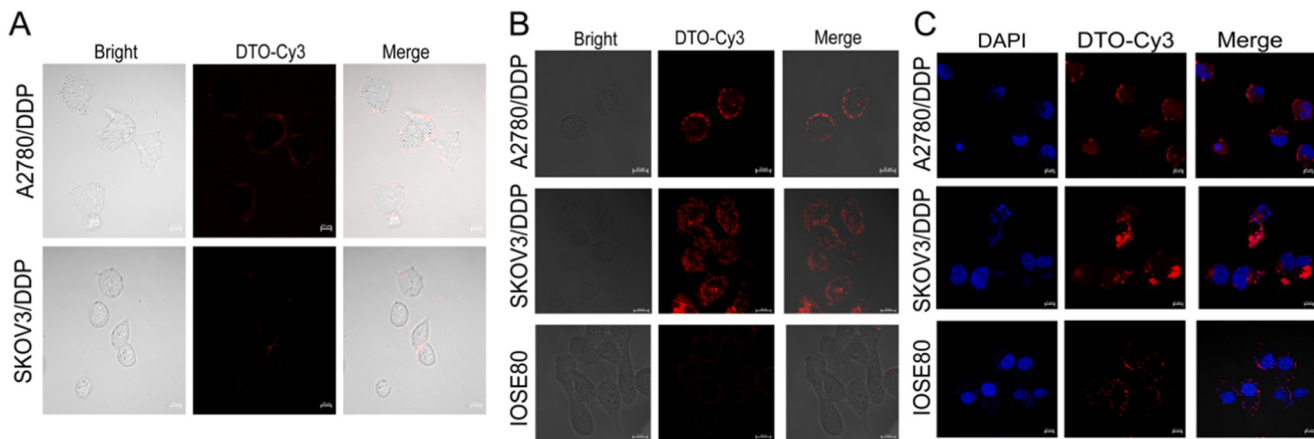


Fig. 8. (A)Real-time capture confocal fluorescence microscope images of the A2780/DDP, SKOV3/DDP cells treated with DTO-Cy3 (100 nM) Scale bar, 10 μ m. (B) Fluorescence images of the A2780/DDP, SKOV3/DDP, IOSE80 cells treated with DTO-Cy3 (100 nM) for 3 h. Scale bar,10 μ m. (C)Fluorescence images of cells treated with DTO-Cy3 (100 nM) for 10 h, fixed with 4% paraformaldehyde and stained with DAPI. Scale bar, 10 μ m.

miR-21 in IOSE80 cells. As is shown, fluorescence accumulates in the cytoplasm of SKOV3/DDP, whereas fluoresces was both on the membrane and in the cytoplasm of A2780/DDP. From this we speculated that under prolonged action, SKOV3/DDP had the strongest uptake of DTO, followed by A2780/DDP, but the opposite was true for short periods of time, which may be related to differences in cell membranes. Interestingly, we observed faint traces of DAPI in the cytoplasm, which could overlap with Cy3. This is because DAPI can bind with high affinity to the DNA minor groove [42]. Therefore, our DTO nanodevice can also be

combined with DAPI. These results indicated that the DTO was indeed internalized by cells and opened. It is found that caveolin-1 (CAV1) is associated with the endocytosis of DNA nanostructures [43,44].

5. Conclusions

In summary, we have constructed a novel DTO nanodevice that opens in response to miR-21 through chain replacement. In contrast to traditional strategies, our DTO is thinner and more compact, which

benefits cellular uptake. The successful construction and switching performance of the DTO were initially verified through extracellular experiments, involving the loading of fluorescence-labeled handle strands into the inner cavity of the DTO. Especially in flow cytometry and real-time fluorescence analyses, A2780/DDP cells achieved cellular uptake in 30 min, indicating that our DTO is extremely simple to internalize by these cells. Live-cell imaging confirmed that the DTO effectively entered ovarian cancer cells that have high expression levels of miR-21. However, due to the lack of targeting, under prolonged incubation, DTO can also be internalized by the normal ovarian epithelial cells IOSE80 and opened by small amounts of miR-21 or through other means. Moreover, in the absence of a fluorescence quencher, it was the change in fluorescence that demonstrated the opening and closing of the DTO.

Our study demonstrates the efficacy of DTO as a viable nanocarrier. The highly editable nature of DNA strands opens avenues for future research focused on drug or siRNA delivery. The inherent morphological and structural qualities of DTO suggest that its internal contents are theoretically more resistant to enzymatic hydrolysis due to the embedding effect. The responsiveness of DTO to miR-21 provides a protective shield for normal cells, mitigating potential toxicity and side effects. The swift internalization and accumulation of DTO could prove advantageous in cancer therapy. To enhance its clinical performance, integrating materials on the outer surface of DTO, such as aptamers or peptides, to increase affinity and targeting ability is a potential avenue for improvement. In summary, our design strategy holds promise for advancing nanodrug development, not only for ovarian cancer but also for numerous other cancer types. Future studies should explore the stability, toxicity, and effectiveness of DTO-based intracellular drug delivery strategies *in vivo*. However, a limitation in our study is the utilization of only one type of normal cell line. To provide a more comprehensive understanding of our research, future work may consider incorporating multiple normal cell lines to assess the generality and applicability of our approach. Such an expansion would contribute to ensuring the universality of our research findings and enhance the understanding of responses in different cellular environments. In conclusion, the intracellular miR-21-initiated chain replacement reaction and the release mechanism of DTO provide new ideas and methods for the delivery of nanoparticles and other fields of precisely controlled release. As technology develops, we believe this mechanism will be more widely used and bring more innovations to fields such as biomedicine and materials science.

Funding

This work was supported by grants from the National Natural Science Foundation of China (No. 62172302).

Author statement

This revised version of the manuscript is based on the comments and suggestions provided by the reviewers and the editor. We have carefully reviewed and addressed each of the suggestions. We believe these revisions will enhance the quality of the paper and improve its contribution to the academic community.

We would like to express our gratitude to the reviewers and the editor for their valuable comments and guidance on our manuscript. We also thank Editage (www.editage.cn) for English language editing. Without their assistance and support, this research would not have been possible.

CRediT authorship contribution statement

Conceptualization: LTH, XL and XLS. Methodology: LTH and XL. Data curation: LTH, TS, XYW, CQG, JDW and ZBW. Writing-Original Draft: LTH. Supervision: XL.

Declaration of Competing Interest

The authors declare that they have no known competing financial interests or personal relationships that could have appeared to influence the work reported in this paper.

Acknowledgments

We would like to thank Editage (www.editage.cn) for English language editing.

Appendix A. Supporting information

Supplementary data associated with this article can be found in the online version at doi:[10.1016/j.csbj.2024.02.021](https://doi.org/10.1016/j.csbj.2024.02.021).

References

- [1] Perez-Herrero E, Fernandez-Medarde A. Advanced targeted therapies in cancer: drug nanocarriers, the future of chemotherapy. *Eur J Pharm Biopharm* 2015;93: 52–79.
- [2] Madsen M, Gothelf KV. Chemistries for DNA nanotechnology. *Chem Rev* 2019;119: 6384–458.
- [3] Rothemund PWK. Folding DNA to create nanoscale shapes and patterns. *Nature* 2006;440:297–302.
- [4] Jungmann R, Scheible M, Simmel FC. Nanoscale imaging in DNA nanotechnology. *Wiley Interdiscip Rev Nanomed Nanobiotechnol* 2012;4:66–81.
- [5] Linko V, Ora A, Kostainen MA. DNA nanostructures as smart drug-delivery vehicles and molecular devices. *Trends Biotechnol* 2015;33:586–94.
- [6] Jiang Q, et al. Rationally designed DNA-origami nanomaterials for drug delivery *in vivo*. *Adv Mater* 2019;31:e1804785.
- [7] Pal S, Rakshit T. Folate-functionalized DNA origami for targeted delivery of doxorubicin to triple-negative breast cancer. *Front Chem* 2021;9:721105.
- [8] Zhang Q, et al. DNA origami as an *in vivo* drug delivery vehicle for cancer therapy. *ACS Nano* 2014;8:6633–43.
- [9] Zhou Y, et al. Self-assembled DNA nanostructure as a carrier for targeted siRNA delivery in glioma cells. *Int J Nanomed* 2021;16:1805–17.
- [10] Baig MMFA, et al. Design, synthesis and evaluation of DNA nano-cubes as a core material protected by the alginate coating for oral administration of anti-diabetic drug. *J Food Drug Anal* 2019;27:805–14.
- [11] Scherf M, et al. Trapping of protein cargo molecules inside DNA origami nanocages. *Nanoscale* 2022;14:18041–50.
- [12] Rothemund PWK, et al. Design and characterization of programmable DNA nanotubes. *J Am Chem Soc* 2004;126:16344–52.
- [13] Li CH, et al. Nucleolin-targeted DNA nanotube for precise cancer therapy through Förster resonance energy transfer-indicated telomerase responsiveness. *Anal Chem* 2021;93:3526–34.
- [14] Wang Z, et al. A tubular DNA nanodevice as a siRNA/chemo-drug co-delivery vehicle for combined cancer therapy. *Angew Chem* 2021;60:2594–8.
- [15] Li Y, et al. Hierarchical assembly of super-DNA origami based on a flexible and covalent-bound branched DNA structure. *J Am Chem Soc* 2021;143:19893–900.
- [16] Ketterer P, Willner EM, Dietz H. Nanoscale rotary apparatus formed from tight-fitting 3D DNA components. *Sci Adv* 2016;2:e1501209.
- [17] Endo M, et al. Helical DNA origami tubular structures with various sizes and arrangements. *Angew Chem* 2014;53:7484–90.
- [18] Stömmer P, et al. A synthetic tubular molecular transport system. *Nat Commun* 2021;12:4393.
- [19] Mohammed AM, Schulman R. Directing self-assembly of DNA nanotubes using programmable seeds. *Nano Lett* 2013;13:4006–13.
- [20] Lee YS, Dutta A. MicroRNAs in cancer. *Annu Rev Pathol* 2009;4:199–227.
- [21] Chai C, et al. MicroRNA-21 promotes glioma cell proliferation and inhibits senescence and apoptosis by targeting SPRY1 via the PTEN/PI3K/AKT signaling pathway. *CNS Neurosci Ther* 2018;24:369–80.
- [22] Hackett EE, et al. Mycobacterium tuberculosis limits host glycolysis and IL-1 β by restriction of PFK-M via microRNA-21. *Cell Rep* 2020;30.
- [23] Liu T, et al. Diagnostic role of circulating MIR-21 in colorectal cancer: a update meta-analysis. *Ann Med* 2021;53.
- [24] Yu Y, et al. MicroRNA-21 regulate the cell apoptosis and cell proliferation of polycystic ovary syndrome (PCOS) granulosa cells through target toll like receptor TLR8. *Bioengineered* 2021;12:5789–96.
- [25] Kuroki I, Guntupalli SR. Treatment of epithelial ovarian cancer. *BMJ (Clin Res Ed)* 2020;371:m3773.
- [26] Colombo N, et al. ESMO-ESGO consensus conference recommendations on ovarian cancer: pathology and molecular biology, early and advanced stages, borderline tumours and recurrent disease†. *Ann Oncol: J Eur Soc Med Oncol* 2019;30: 672–705.
- [27] Lheureux S, et al. Epithelial ovarian cancer. *Lancet* 2019;393:1240–53.
- [28] Chen X, et al. lncRNA mortal obligate RNA transcript was downregulated in ovarian carcinoma and inhibits cancer cell proliferation by downregulating miRNA-21. *J Cell Biochem* 2019;120:11949–54.

- [29] Au Yeung CL, et al. Exosomal transfer of stroma-derived miR21 confers paclitaxel resistance in ovarian cancer cells through targeting APAF1. *Nat Commun* 2016;7:11150.
- [30] Liu HY, et al. miR-21 regulates the proliferation and apoptosis of ovarian cancer cells through PTEN/PI3K/AKT. *Eur Rev Med Pharmacol Sci* 2019;23:4149–55.
- [31] Liu H, Hong F, Smith F, Goertz J, Ouldridge T, Stevens MM, et al. Kinetics of RNA and RNA:DNA hybrid strand displacement. *ACS Synth Biol* 2021;10(11):3066–73.
- [32] Douglas SM, et al. Rapid prototyping of 3D DNA-origami shapes with caDNAno. *Nucleic Acids Res* 2009;37:5001–6.
- [33] Woods D, et al. Diverse and robust molecular algorithms using reprogrammable DNA self-assembly. *Nature* 2019;567:366–72.
- [34] Albanese, A., et al. The effect of nanoparticle size, shape, and surface chemistry on biological systems. *Annual Review of Biomedical Engineering*, 14, 1–16.
- [35] Xue C, et al. Programmably tiling rigidified DNA brick on gold nanoparticle as multi-functional shell for cancer-targeted delivery of siRNAs. *Nat Commun* 2021;12:2928.
- [36] Si ML, et al. miR-21-mediated tumor growth. *Oncogene* 2007;26:2799–803.
- [37] Frezzetti D, et al. Upregulation of miR-21 by Ras in vivo and its role in tumor growth. *Oncogene* 2011;30:275–86.
- [38] An Y, Yang Q. MiR-21 modulates the polarization of macrophages and increases the effects of M2 macrophages on promoting the chemoresistance of ovarian cancer. *Life Sci* 2020;242:117162.
- [39] Schüller VJ, et al. Cellular immunostimulation by CpG-sequence-coated DNA origami structures. *ACS Nano* 2011;5:9696–702.
- [40] Ko S, et al. DNA nanotubes as combinatorial vehicles for cellular delivery. *Biomacromolecules* 2008;9:3039–43.
- [41] Wang P, et al. Visualization of the cellular uptake and trafficking of DNA origami nanostructures in cancer cells. *J Am Chem Soc* 2018;140:2478–84.
- [42] Farahat AA, et al. Exploration of DAPI analogues: synthesis, antitrypanosomal activity, DNA binding and fluorescence properties. *Eur J Med Chem* 2017;128:70–8.
- [43] Tian T, Zhang C, Li J, Liu Y, Wang Y, Ke X, et al. Proteomic exploration of endocytosis of framework nucleic acids. *Small* 2021;17(23):e2100837.
- [44] Nishikawa M, Tan M, Liao W, Kusamori K. Nanostructured DNA for the delivery of therapeutic agents. *Adv Drug Deliv Rev* 2019;147:29–36.